Josephson modulation of the critical current in $YBa_2Cu_3O_{7-\delta}$ films

P. Bernstein, Y. Bougherira, J. F. Hamet, and Y. Thimont
CRISMAT (UMR-CNRS 6508)-ENSICAEN and Université de Caen-Basse Normandie, Boulevard du Maréchal Juin, F14050 Caen Cedex, France

L. Méchin
GREYC (UMR-CNRS 6072)-ENSICAEN and Université de Caen-Basse Normandie, Boulevard du Maréchal Juin, F14050 Caen Cedex, France

(Received 6 February 2008; revised manuscript received 28 July 2008; published 22 August 2008)

Assuming that the boundary planes in $YBa_2Cu_3O_{7-\delta}$ can show a Josephson behavior, we establish the conditions required in epitaxial thin films to observe the modulation of the critical current by an applied magnetic field, as well as the possible forms of the modulated current. We report measurements carried out on two $YBa_2Cu_3O_{7-\delta}$ films in the near vicinity of the critical temperature that show a partial modulation of their critical current. The comparison of the measured critical current changes to those predicted by the calculations shows that the experimental results are consistent with the Josephson modulation of the current carried by associations of weak links located in the boundary planes.

DOI: 10.1103/PhysRevB.78.054517 PACS number(s): 74.50.+r, 74.78.Bz, 74.25.Sv

I. INTRODUCTION

The suggestion that boundary planes, especially the low angle grain boundaries (LAGBs) and the twin boundaries (TBs) play an important role in the properties of *c*-axis $YBa_2Cu_3O_{7-\delta}$ (YBCO) films, has been proposed for a long time.[1–3] Since their width is in the range of $\xi_{ab}(T)$, the superconducting coherence length in the *a*-*b* planes of YBCO, many authors have presumed some type of Josephson coupling across the boundary planes. Deutscher[1,2] proposed that they behave as Josephson junctions with a depressed order parameter. Mezzetti *et al.*[4] regarded them as long Josephson junctions whose coupling energy is modulated by defects. Gurevich and Colley[5,6] considered that the vortices whose cores are located on the boundary planes are Abrikosov vortices with Josephson cores, they have called Abrikosov-Josephson vortices. An expected consequence of Josephson coupling is the modulation of the critical current by a magnetic field. This phenomenon has been predicted in highly anisotropic cuprates, as resulting from the intrinsic Josephson coupling between CuO_2 layers.[7] In ceramic materials, the strong sensitivity of the critical current to an applied field has been attributed to the combined Josephson behavior of the multiple weak links connecting the grains.[8,9] In YBCO films, modulation of the critical current has been obtained either in nanobridges[10,11] or by creating artificial grain boundaries with some angle either between domains with the same basal plane[12–14] or between domains with different basal planes.[15,16] However, no phenomenon of this type has been reported so far in YBCO thin films patterned in geometries of micrometric size including natural boundary planes only.

In previous papers, we have suggested that, due to the numerous defects they include, the TBs in YBCO split off into rows of Josephson weak links whose physics, when no field is applied, determines the critical current and other properties of the films.[17–19] A consequence of this model is that the modulation of the critical current of the films should be observed in the vicinity of the critical temperature. In this paper, we detail this point and we report the measurements carried out on thin-film microbridges.

In Sec. II of the paper we remind of some of the aspects of our model relevant for this work and we establish the conditions required to observe the Josephson modulation of the critical current in YBCO thin films. In Sec. III, we detail the characteristics and making process of the studied samples and the measurement techniques. The experimental results are reported in Sec. IV and discussed in Sec. V.

II. PROPERTIES OF YBCO FILMS IN THE CRITICAL STATE WITH NO APPLIED FIELD AND CONDITIONS FOR THE OBSERVATION OF THE JOSEPHSON MODULATION OF THE CRITICAL CURRENT

In this section we first summarize some features of the model we have developed for *c*-axis YBCO epitaxial films in the critical state with no applied magnetic field.[17–19] The model is valid for films whose thickness is in the range of or smaller than $2\lambda_{ab}$ (λ_{ab} is the superconducting penetration depth in the *a*-*b* planes of YBCO). In the second part of this section, we examine the conditions in which some of the Josephson weak links included in the films boundary planes can cause the modulation of the sample critical current when a low magnetic field is applied and we discuss the possible expressions of the modulated current.

A. Critical state of YBCO films with no applied magnetic field

As other authors,[1–6] we assume that when a superconducting current flows parallel to the *a*-*b* planes of YBCO films, a tunneling pair current flows between the superconducting banks of the boundary planes parallel to the *c* axis. In previous works, we have assumed that the TBs play the main role in epitaxial films. We will take a more general view in this contribution. As a starting point, we consider the consequences of the existence along the boundary planes of defects with a size in the range of or smaller than $\xi_{ab}(T)$. In the case of the TBs, as revealed by high-resolution electron microscopy (HREM) observations, these defects correspond to

tiny atomic displacements, variation in atoms coordination, or local vacancies.[20,21] The average size of this disorder is three cells in the *a-b* planes for the most coherent TBs. In addition, the existence of TBs is associated with a lattice rotation that is not exactly 90° but 89.1°, which implies a lattice distortion and strain fields at the TBs locations that locally change the TBs width. Microscopic observations of grain boundaries with various angles have shown that the dislocations are formed either on the Y/Ba sublattice or on the Cu sublattice, where they affect the formation of charge carrying holes.[22] This results in the existence of charge-carrier depletion layers in the grain boundaries due to copper sites that are undercoordinated to O atoms. The existence of these defects suggests that the separation between the boundary planes superconducting banks can be locally large enough, with respect to $\xi_{ab}(T)$, to cause a disruption of the tunneling current. This observation has led Mezzetti *et al.*[4] to consider that the boundary planes include separate subjunctions carrying the same Josephson current density but showing statistically distributed lengths (along the boundary planes). Taking a slightly different point of view, we assume that the boundary planes split off into rows of Josephson weak links whose length depends on the temperature.[17] We now consider the current and magnetic-flux penetration when a bias current is injected in a thin film. Magneto-optical observations on a strip have shown that vortices and antivortices enter progressively from the opposite edges of the sample, while the central zone remains flux free and carries a low current density.[23] The area of the flux free zone decreases as the current increases, and the film is in the critical state when this region disappears. Then, in spite of pinning and as an effect of thermal activation, vortices and antivortices move in the direction of the middle of the film where they annihilate each other. In addition, magneto-optical observations on a single crystal have shown that the TBs are the first areas penetrated by the magnetic flux.[24] Then, it is reasonable to assume that in thin films, in the region penetrated by the flux, the vortices and antivortices are preferentially located along the boundary planes that they fill up in the critical state. The distinctive point of our model is that we take into account the small size defects that exist in the boundary planes, but that are not large enough to cause a disruption of the tunneling current at the measurement temperature. They are included in the weak links and we can expect that, in the critical state, they limit the pair coupling current to the lowest value maintaining the phase coherence across the boundary planes against thermal fluctuations. As a result, we assume that the weak link energy is equal to $k_B T$ and that all the weak links (except those located at the vortex cores) carry the same net current that is equal to

$$I_J = \frac{2\pi k_B T}{\phi_o}, \tag{1}$$

where ϕ_o is the flux quantum. Current $I_J(T)$ and the weak links mean length along the boundary planes, $\bar{\delta}(T)$, have been experimentally determined for various films.[19] Length $\bar{\delta}(T)$ was estimated from the curvature of the current-voltage curves measured on microbridges and was found to obey the empirical law,

$$\bar{\delta} = \delta_o \left(1 - \frac{T}{T_c}\right)^{-3/2}, \tag{2}$$

where $\delta_o = 0.55$ nm and T_c is the offset critical temperature. Since the mean weak link length cannot be less than the mean distance between the electrons of a Cooper pair, the validity of Eq. (2) is limited to the temperature domain for which $\bar{\delta}(T)$ is larger than $\xi_{ab}(T)$, i.e., above a low-temperature limit, T_{low}. Current $I_J(T)$ was determined by dividing the microbridge critical current by the mean number of weak links located in a boundary plane. It has turned out that Eq. (1) is verified between T_{low} and a maximum temperature, T_{up}. Between T_{up} and T_c, the experimental $I_J(T)$ curves behave as decreasing functions. We have suggested that this behavior is due to the growing number of weak links that enter a nonsuperconducting state as the temperature increases above T_{up}, while the superconducting weak links still carry current I_J as given by Eq. (1).[18]

B. Josephson modulation of the critical current

The reason that no magnetic modulation of the pair tunneling current across natural boundary planes has been observed so far in YBCO microbridges or strips is that there is no coherence over a long distance in Ψ, the phase difference between the two banks of a given boundary plane. This is due mainly to the existence of vortex cores in the boundary planes that causes discontinuities in Ψ. Then, ℓ_c, the coherence length in Ψ, extends over a distance at most equal to the distance between two vortex cores. As a result, for $T < T_{\text{up}}$, the boundary planes behave as collections of Josephson weak links with various lengths that respond incoherently to the magnetic field and there is no modulation of the critical current.

For $T > T_{\text{up}}$, according to our model, the boundary planes include structures consisting of superconducting and nonsuperconducting weak links. The simplest structures either include $2n_c$ superconducting weak links and n_{ns} nonsuperconducting ones, as sketched in Fig. 1(a), or consist of n_c successive superconducting weak links, as shown in Fig. 1(b). If, along the boundary planes, there is a sufficient number of identical structures of one or the other type shorter than ℓ_c, they can respond coherently to the magnetic field and cause the modulation of a fraction of the critical current. We first assume that the length of all the weak links located along the boundary planes is equal to $\bar{\delta}$. Considering the structure of Fig. 1(a), the current that flows across the superconducting weak links takes the form,

$$I_S(B) = n_c I_J \left[\int_{y_1 - n_c \bar{\delta}/2}^{y_1 + n_c \bar{\delta}/2} \sin \Psi dy + \int_{y_2 - n_c \bar{\delta}/2}^{y_2 + n_c \bar{\delta}/2} \sin \Psi dy \right], \tag{3}$$

with

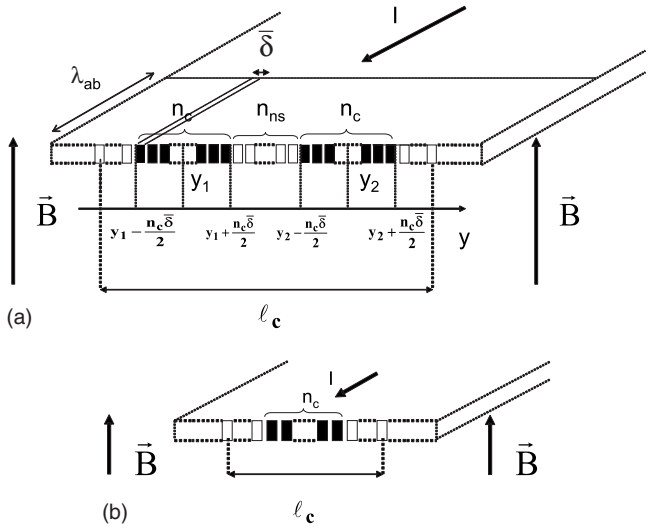

FIG. 1. Sketches of two structures consisting of superconducting (black squares) and nonsuperconducting weak links (white squares) included in a weak links row inside a boundary plane near T_c. These structures can respond coherently to an applied magnetic field because their length is shorter than ℓ_c, the coherence length of the phase difference between the two banks of the boundary plane; (a) SQUID-like structure consisting of $2n_c$ superconducting weak links and n_{ns} nonsuperconducting ones; (b) structure consisting of n_c superconducting weak links neighboring nonsuperconducting ones.

$$\Psi(y) = \Psi(y_1) + (y - y_1)\frac{4\pi\lambda_{ab}B}{\phi_o}, \tag{4}$$

and

$$y_2 = y_1 + (n_c + n_{ns})\bar{\delta}. \tag{5}$$

The calculation of $I_S(B)$ yields

$$I_S(B) = 2n_c I_J \frac{\sin\left(\frac{n_c\pi\Phi}{\phi_o}\right)}{\frac{n_c\pi\Phi}{\phi_o}}\cos\left[(n_c + n_{ns})\frac{\pi\Phi}{\phi_o}\right] \times \sin\left[\Psi(y_1) + (n_c + n_{ns})\frac{\pi\Phi}{\phi_o}\right], \tag{6}$$

where

$$\Phi = 2\lambda_{ab}\bar{\delta}B \tag{7}$$

is the magnetic flux across one weak link. Considering that there is no other superconducting weak link over distance ℓ_c, the maximum value of current $I_S(B)$ is that for which

$$\Psi(y_1) = \pm\frac{\pi}{2} - (n_c + n_{ns})\frac{\pi\Phi}{\phi_o}, \tag{8}$$

and $I_S(B)$ takes the form,

$$I_S(B) = I_S(0)\left|\frac{\sin\left(\frac{n_c\pi\Phi}{\phi_o}\right)}{\frac{n_c\pi\Phi}{\phi_o}}\cos\left[(n_c + n_{ns})\frac{\pi\Phi}{\phi_o}\right]\right|. \tag{9}$$

Equation (9) is very similar to that giving the current flowing across a superconducting quantum interference device (SQUID) in which the junction size is significant with respect to the size of the loop. The current flowing across the simple structure in Fig. 1(b) is derived straightforward from Eq. (9). We have

$$I_S(B) = I_S(0)\left|\frac{\sin\left(\frac{n_c\pi\Phi}{\phi_o}\right)}{\frac{n_c\pi\Phi}{\phi_o}}\right|. \tag{10}$$

Equations (9) and (10) account for the contribution to the critical current of modulating structures similar to that sketched, respectively, in Figs. 1(a) and 1(b). If the other weak links along the boundary planes do not respond coherently to the application of the modulating field, for example, because they are included in structures longer than ℓ_c, the critical current can be written as

$$I_{cr}(B) = I_M(B) + I_{BG} \tag{11}$$

In Eq. (11) I_{BG} is a background current and $I_M(B)$ shows a dependence on B similar to that of $I_S(B)$ either in Eq. (9) or in Eq. (10). However, we can discard neither the possibility that there is some scattering in the weak links lengths nor that in addition to the structures responsible for the most part of the response of the sample, there are other modulating structures along the boundary planes that contribute to $I_{cr}(B)$. Then, we must consider that the response can be that of a disordered system. In the case of classical Josephson junctions with spatial fluctuations that can be described with the Poisson distribution, Barone and Paterno[25] proposed the expression,

$$I_{cr}(B) = \left[I_{cr}^2(0)\left[\frac{\sin\left(\frac{\pi\Phi^*}{\phi_o}\right)}{\frac{\pi\Phi^*}{\phi_o}}\right]^2 + I_{BG}^2\left\{1 - \left[\frac{\sin\left(\frac{\pi\Phi^*}{\varphi_o}\right)}{\frac{\pi\Phi^*}{\phi_o}}\right]^2\right\}\right]^{1/2}, \tag{12}$$

to account for the resulting critical current modulation. In Eq. (12), Φ^* is the magnetic flux across the junction. By analogy, assuming that the superconducting weak links distribution obeys a probability law not strongly different from the Poisson's law, we propose that Eq. (12) accounts for the response of disordered boundary planes including simple structures of the type shown in Fig. 1(b). Then, in Eq. (12), we write $\Phi^* = n_c\Phi$, where n_c is the most probable number of superconducting weak links in the modulating structures.

TABLE I. Substrate, buffer layer, thickness d, and offset (respectively onset) critical temperature T_c (respectively T_{con}) of the investigated samples.

	Substrate	Buffer layer	d (nm)	T_c (K)	T_{con} (K)
G120B	MgO	none	245	84.4	84.8
G123B	MgO	$SrTiO_3$	120	89.7	91.5

From a general point of view, we expect that the measurements for which Eq. (12) gives good fittings will correspond to large n_c values since a large number of structures with a number of superconducting weak links different from n_c will contribute to $I_{cr}(B)$. At the opposite, if n_c is low, Eq. (12) can be ill-suited and Eqs. (10) and (11) give a better fitting. We will compare the expressions of $I_{cr}(B)$ obtained in this section with the experimental measurements in Sec. IV.

III. EXPERIMENT

A. Samples

We have investigated the electrical properties of two laser ablated YBCO films. Film G120B was deposited on a MgO substrate and film G123B was deposited on a MgO substrate coated with a 6-nm-thick $SrTiO_3$ (STO) buffer layer. Both YBCO and STO layers were grown by Krypton-fluor pulsed laser deposition from stoichiometric targets onto the substrates. The 10×5 mm^2 substrates were clamped in front of a resistive heater and were radiantly heated from the backside. The laser radiation energy density was 1.5 J cm^{-2} for YBCO and 2 J cm^{-2} for STO. A comprehensive x-ray diffraction study led to the optimized deposition temperature of 700 °C for both materials and to the optimized O_2 pressures of 0.5 and 0.3 mbar for YBCO and STO, respectively. Right after deposition, a 700 mbar oxygen pressure was introduced in the deposition chamber and the films were cooled to ambient temperature at 20 °C min^{-1} including a 30 min plateau at 500 °C. Full c-axis oriented YBCO films were thus obtained. The main properties of the films are reported in Table I. The sample with the STO buffer layer (film G123B) has a critical temperature higher than the film directly deposited on MgO. For this last one, the large difference between the in-plane lattice parameter of MgO (a=0.421 nm) and those of YBCO (a=0.382 nm and b=0.388 nm) has effects upon the epitaxial growth of the film. As sketched in Fig. 2, the film growth occurs either by direct epitaxy (growth of domains whose [100] axis are parallel to the [100] axis of MgO) or by indirect epitaxy (growth of domains whose [100] axis are parallel to the [110] axis of MgO). The critical temperature of the obtained films is reduced with respect to the optimal one. A STO buffer layer grows on MgO with its [100] axis parallel to the [100] axis of MgO and enables the direct epitaxy of a high critical temperature YBCO film.[26,27]

After deposition, the films were patterned as microbridges with various dimensions using contact UV photolithography and argon ion milling. The measurements presented here were carried out on 300×10 μm^2 microbridges.

B. Electrical measurements

For the electrical measurements, the microbridges were inserted in a cryocooler. A solenoid external to the cryocooler could create a perpendicular magnetic field $B \leq 10$ mT at the sample level. The current-voltage characteristics of the microbridges were measured in the vicinity of T_c in the four-point configuration method using a 553 Hz alternating current, maintaining the temperature fluctuations in the ±0.01 K range. The measurements were averaged over a large number of data acquisitions in order to eliminate the noise due to the cryocooler. Other details on the measurement technique can be found in Ref. 19.

C. Determination of the critical current

In the vicinity of the critical state, the vortex motion in YBCO films is thermally activated. The expression,

$$V = R_A(I - I_{cr})\sinh\left(\frac{I}{I_o}\right), \tag{13}$$

where I_{cr} is the threshold current for $V\neq0$, and R_A and I_o are the other fitting parameters, was proposed in Refs. 17–19 for fitting the current-voltage characteristics measured with $B=0$. This expression has enabled us to determine I_{cr} with a better accuracy than a voltage criterion. For $B\neq0$, the validity of Eq. (13) is not established from the point of view of the physics. Nevertheless, we have observed that this equation was also a good fitting function when the measurements were carried out with a weak applied field and provided an accurate estimation of the critical current. The reason is probably that in these conditions R_A and I_o show little changes with respect to their zero-field values. As a consequence, we have taken Eq. (13) as an *ad hoc* fitting function to determine $I_{cr}(B)$.

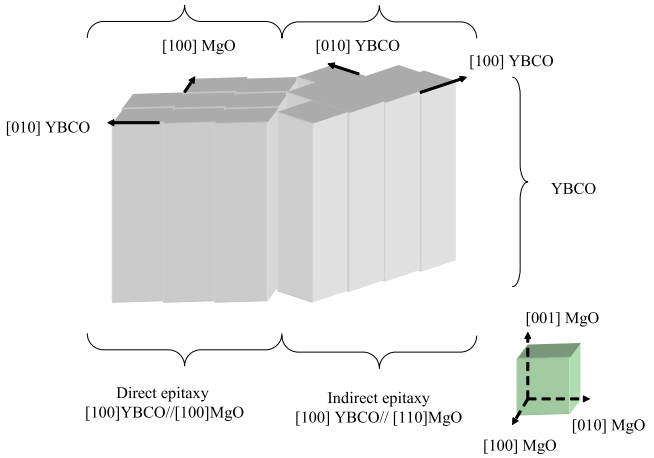

FIG. 2. (Color online) Sketch of the YBCO domains that grow on MgO substrates. In case of direct epitaxy, the [100] axis of YBCO is parallel to the [100] axis of MgO while for indirect epitaxy it is parallel to the [110] axis of MgO.

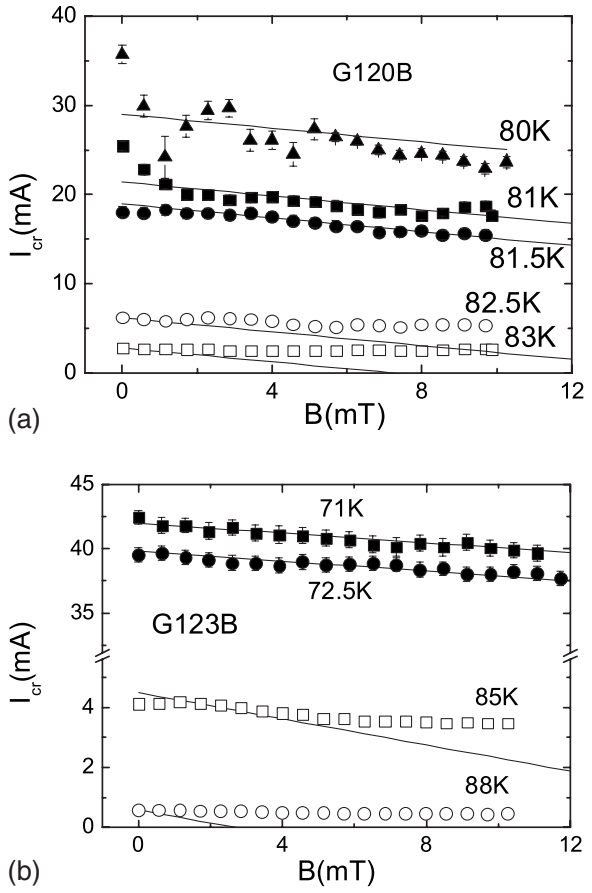

FIG. 3. Critical current of microbridges (a) G120B and (b) G123B, as a function of the amplitude of the external field, B, at various temperatures. The solid lines are calculated with the relation $I_{\rm cr}(B)=I_{\rm cr}(0)-2dB/\mu_o$ [Eq. (17)].

IV. RESULTS

We have recorded the current-voltage characteristics of the two microbridges at various temperatures and magnetic-field amplitudes. Figures 3(a) and 3(b) show $I_{\rm cr}(B)$ for microbridges G120B and G123B, respectively. In the lowest-temperature range $I_{\rm cr}(B)$ is a decreasing linear function. We observe a different behavior in the near vicinity of T_c. The linear regime is discussed in Sec. V A. Here we will focus on the measurements carried out near T_c. The $I_{\rm cr}(B)$ curves measured near T_c and shown in Figs. 4–6 on a dilated scale suggest that a fraction of the critical current is modulated by the magnetic field. In what follows, we compare these measurements with calculations made with Eqs. (9)–(11) on the one hand and with Eq. (12) on the other hand. For this purpose, we need to determine $\lambda_{ab}(T)$. In principle, since the measurements were carried out in the vicinity of the critical temperature, this length can be calculated with the Ginzburg-Landau expression. Another expression can be obtained from the two-fluid model. However, high-frequency experiments have shown that $\lambda_{ab}(T)$ in YBCO is more accurately reproduced with the relation,[28,29]

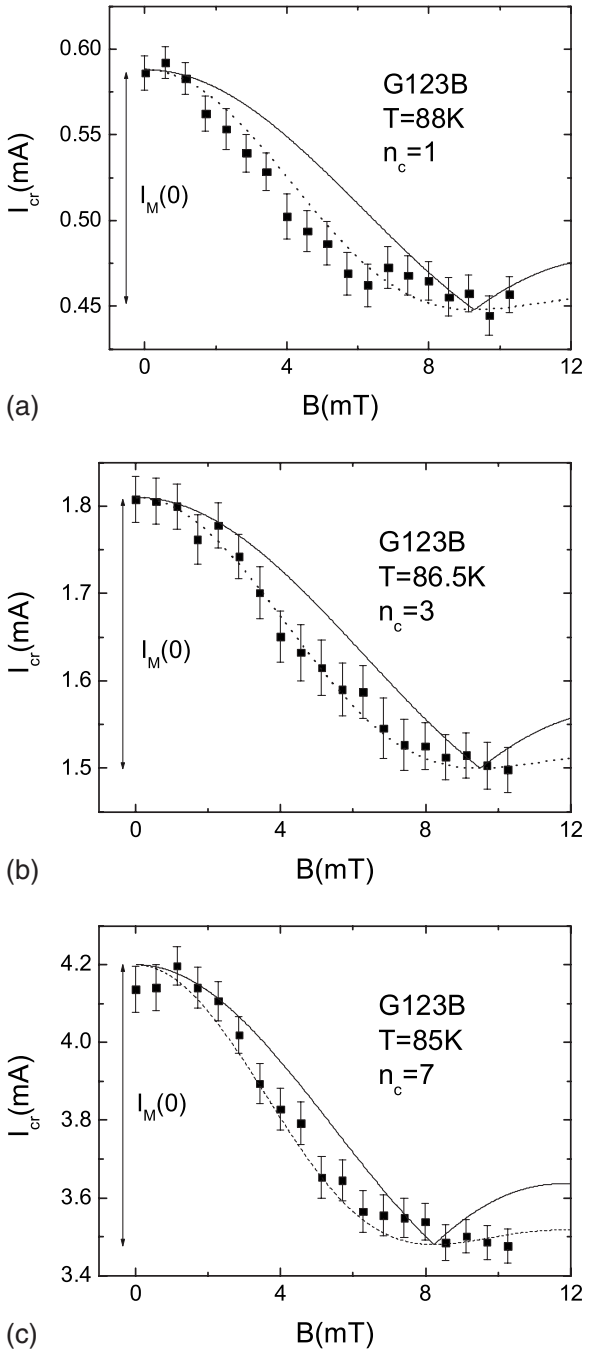

FIG. 4. Critical current of microbridge G123B as a function of the applied magnetic field at (a) $T=88$, (b) 86.5, and (c) 85 K. The solid lines are calculated with Eqs. (10) and (11), while the dotted lines are calculated with Eq. (12), taking for n_c the values reported in the figures. At each measurement temperature, the amplitude of the modulated fraction of the critical current, $I_M(0)$, is determined as shown.

$$\lambda_{ab}\left(\frac{T}{T_{c_{\rm on}}}\right)=\lambda_{ab}(0)\left[1-\left(\frac{T}{T_{c_{\rm on}}}\right)^2\right]^{-1/2}. \qquad (14)$$

The zero-temperature penetration depth cannot generally be determined from these measurements. We will take $\lambda_{ab}(0)=145$ nm, which is in the average range found in the litera-

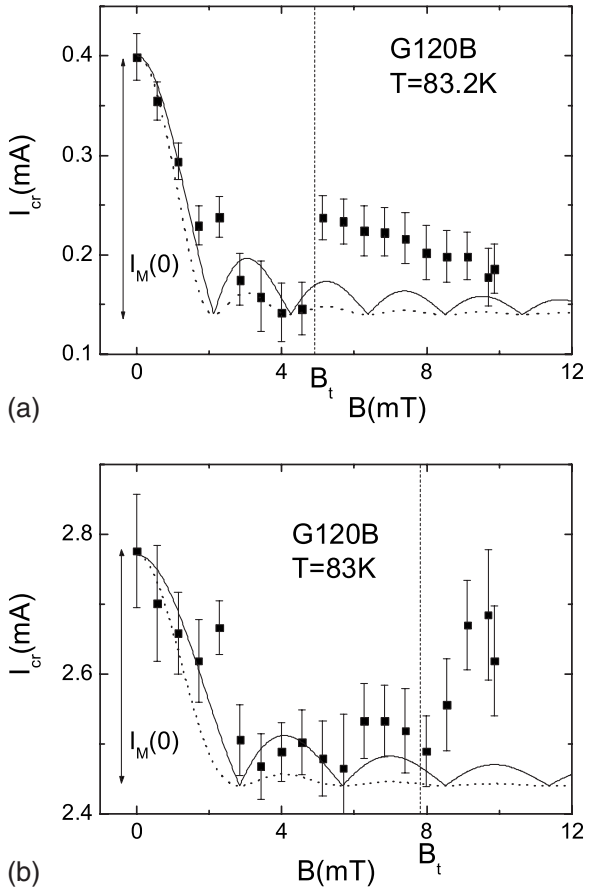

FIG. 5. Critical current of microbridge G120B as a function of the applied magnetic field at (a) $T=83.2$ and (b) 83 K. The solid lines are calculated with Eqs. (10) and (11), while the dotted lines are calculated with Eq. (12), taking $n_c=2$. $I_M(0)$ is determined as shown in the figures. B_t is the field value above which the length of the modulating structures is larger than the mean distance between vortex cores.

ture. In Eq. (14), $T_{c_{on}}$ is the onset critical temperature. This temperature is reported in Table I for both microbridges.

For microbridge G123B [Figs. 4(a)–4(c)] no fitting of $I_{cr}(B)$ with Eqs. (9) and (11), which correspond to the SQUID-like structures sketched in Fig. 1(a), is possible. Taking for n_c the values reported in the figures, the fitting curves calculated with Eq. (12) (dotted lines), which account for a large disorder along the boundary planes, are in a much better agreement with the experimental points than those calculated with Eqs. (10) and (11) (solid lines). This suggests that the weak links distribution in the simple structures located along the boundary planes of microbridge G123B is at least unimodal, with n_c as both most probable and mean value (except at $T=88$ K, since $n_c=1$ cannot be exactly the mean value of the weak links distribution). It is interesting to compare the dependence on temperature of n_c with that of the mean number of superconducting weak links located in a boundary plane, $\bar{N}_c=I_{cr}(0)/I_J$. Table II shows that $\bar{N}_c/n_c$, that is the mean number of structures carrying successive superconducting weak links in a boundary plane takes almost the same value at the three measurements temperatures. The consequences of this result are discussed in Sec. V C.

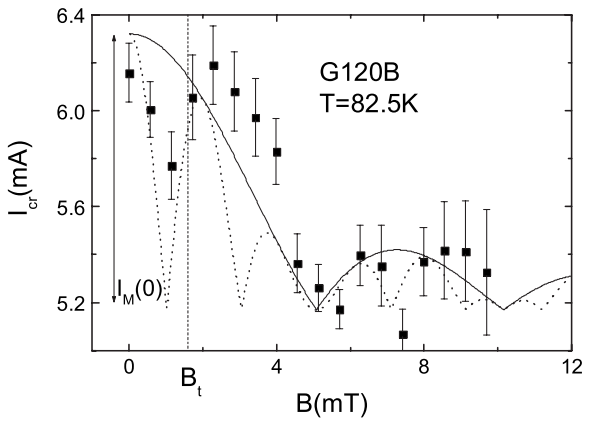

FIG. 6. Critical current of microbridge G120B as a function of the applied magnetic field at 82.5 K. The dotted line is calculated with Eqs. (9) and (11) taking $n_c=2$ and $n_{ns}=3$, while the solid line is calculated with Eqs. (10) and (11), taking $n_c=2$. The quantity $I_M(0)$ is determined as shown in the figure. B_t is the field value above which the length of the SQUID-like structure with $n_c=2$ and $n_{ns}=3$ is larger than the mean distance between vortex cores.

The measurements carried out on microbridge G120B suggest that the modulation is due to simple structures with $n_c=2$ at $T=83.2$ and 83 K [Figs. 5(a) and 5(b)]. At $T=83.2$ K the experimental points can be fitted either with Eqs. (10) and (11) or with Eq. (12) although the measurements for $B>5$ mT are reproduced with none of the models [see Fig. 5(a)]. The measurements at $T=83$ K [Fig. 5(b)] are clearly better reproduced with Eqs. (10) and (11) (solid line) than with Eq. (12) (dotted line), which does not account for the bumps at $B\approx4$ and 7 mT. However, none of the models accounts for the strong $I_{cr}(B)$ increase above 8 mT. The measurements carried out at $T=82.5$ K can be either reproduced with the equations of the SQUID-like structures [Eqs. (9) and (11)] taking $n_c=2$ and $n_{ns}=3$, which result in the dotted line in Fig. 6, or with that corresponding to simple structures with $n_c=2$ [Eqs. (10) and (11)], which give the solid line. Equations (9) and (11) predict a minimum at 3 mT that is not observed in the experimental results and calculations with Eqs. (10) and (11) do not account for the first experimental minimum at 1.1 mT. The failures of the models at the three measurement temperatures are discussed in Sec. V.

V. DISCUSSION

In this section, we first discuss the behavior of $I_{cr}(B)$ in the low-temperature range of the measurements. We examine the reasons why the models fail to reproduce some of the measurements carried out on microbridge G120B. We compare the $I_{cr}(B)$ curves and the $\bar{N}_c/n_c$ dependence on temperature of both microbridges and we discuss the nature of their modulating boundary planes. At last, we compare the behavior of the investigated microbridges with that of samples including artificial grain boundaries.

A. Behavior of $I_{cr}(B)$ in the lower-temperature range

Assuming that the films enter the critical state when the Lorentz force due to the bias current is equal to the pinning

TABLE II. Most probable number, n_c, of successive superconducting weak links included in the modulating structures of the microbridges at temperature T and ratio $\bar{N}_c/n_c$, where $\bar{N}_c$ is the mean number of superconducting weak links included in a boundary plane.

	G123B			G120B	
T (K)	n_c	$\bar{N}_c/n_c$	T (K)	n_c	$\bar{N}_c/n_c$
88	1	159	83.2	2	57
86.5	3	166	83	2	399
85	7	166	82.5	2	878

force acting on the vortices located on the boundary planes, Gurevich and Colley[6] have claimed that $I_{cr}(B)$ is an increasing function at low fields. Albrecht *et al.*[30] have come to the same conclusion from magneto-optical observations of the magnetic-flux penetration in artificial LAGBs. This prediction was not verified by measurements carried out by Mezzetti *et al.*,[4] and Figs. 3(a) and 3(b) show that it is also not verified on microbridges G120B and G123B. We can account for the linear decrease in $I_{cr}(B)$ if we suppose that the microbridges enter the critical state when the sum of the applied and self-fields along one edge of the microbridge is equal to a critical value. As shown in Ref. 17, the modulus of the self-field along the samples edges takes the form,

$$B_{sf}^{edge} = \frac{\mu_o I}{2d}, \tag{15}$$

where d is the film thickness. Then, the critical field is obtained from the zero applied field critical current as $B_{cr} = \mu_o I_{cr}(0)/2d$, and we can write

$$B = B_{cr} - B_{sf}^{edge} = \frac{\mu_o[I_{cr}(0) - I_{cr}(B)]}{2d}, \tag{16}$$

which is equivalent to

$$I_{cr}(B) = I_{cr}(0) - \frac{2dB}{\mu_o}. \tag{17}$$

The $I_{cr}(B)$ values computed with Eq. (17) are shown as solid lines in Figs. 3(a) and 3(b) and are in good agreement with the measurements in the considered temperature ranges.

B. Failures of the models on microbridge G120B

As seen in Sec. II, critical current modulation is possible if the length of the modulating structures l_{st} is smaller than the coherence length in Ψ. The upper limit for this length is the intervortex distance d_ϕ that takes the form $d_\phi \approx \sqrt{\phi_o/B}$ in the central region of the microbridges, where the self-field is almost zero. As a consequence, no modulation can occur for $B > B_t$, where B_t is obtained from the relation $l_{st} = \sqrt{\phi_o/B_t}$. At $T=83.2$ and 83 K, since the modulation is attributed to simple structures with $n_c=2$, the length of the modulating structures is $l_{st}(T) = 2\bar{\delta}(T)$, which yields $B_t \approx 4.9$ mT at $T=83.2$ K and $B_t \approx 7.8$ mT at $T=83$ K. It is clear from Figs. 5(a) and 5(b) that these values are the threshold fields for the fitting breakdowns at the considered temperatures. At $T=82.5$ K, the low-field behavior of the microbridge is well reproduced supposing that the modulating structures consist of SQUID-like structures with $n_c=2$ and $n_{ns}=3$ (Fig. 6). The length of these structures is $l_{st}=7\bar{\delta}$, which corresponds to $B_t \approx 1.6$ mT. The measurements above B_t are fairly well reproduced assuming that the modulating structures include two successive weak links only. This suggests strongly that the SQUID-like structures modulating the critical current at low field are downgraded to simple structures with $n_c=2$ above B_t.

The above considerations are supported by the results obtained with microbridge G123B that show no fitting breakdown, while the condition $l_{st} < \sqrt{\phi_o/B}$ is fulfilled for all the measurements carried out on this microbridge.

C. $I_{cr}(B)$ curves and the modulating structures of the films

The $I_{cr}(B)$ measurements carried out on microbridge G123B can only be reproduced with Eq. (12), which assumes a large disorder in the boundary planes. As mentioned above, there is a sizable difference between d_ϕ and l_{st} in the whole range of the measurements carried out on this sample. In addition, except at 88 K, we have $n_c > 2$. Then, a large number of modulating structures with a number of superconducting weak links different from n_c contribute probably to $I_{cr}(B)$. For microbridge G120B, we have $n_c=2$ and the difference between d_ϕ and l_{st} is less important since we have $d_\phi - l_{st} > 0$ below B_t only. Then, the only other modulating structures consist probably of single weak links, which is the reason that the $I_{cr}(B)$ curves can be fitted with Eqs. (9)–(11).

The mean number of structures carrying successive superconducting weak links along the boundary planes of microbridge G123B, as given by the ratio $\bar{N}_c/n_c$ in Table II, shows almost no dependence on the temperature. This suggests that above T_{up}, as the temperature increases, the extent of the sections that remain superconducting along the boundary planes decreases, while their number remains almost unchanged. A possible reason could be that these sections consist of cores with a high critical temperature surrounded by regions whose critical temperature decreases as the distance to the core increases. At the opposite, Table II shows that the ratio $\bar{N}_c/n_c$ for film G120B decreases strongly as the temperature increases. This suggests that above T_{up} the modulating structures are located on superconducting islands whose critical temperature is scattered between T_{up} and T_c. As a result of the growth process discussed in Sec. III A, YBCO

films deposited on MgO include boundary planes between domains with the same orientation on the one hand and boundary planes between [100] and [110] domains on the other hand. Since their presence results in a reduction in T_c, we can presume that superconductivity in the boundary planes located between [100] and [110] domains is weaker than in those located between domains with the same orientation. We expect then that nonsuperconducting weak links appear first in these boundary planes and that they carry the modulating structures of film G120B.

As a conclusion, the differences in the $I_{cr}(B)$ curves between the two microbridges arise probably from the fact that the modulating structures are located on different types of boundary planes. They are carried by the strongly superconducting boundary planes between [100] domains in film G123B, while they are probably carried by the boundary planes with a weaker superconductivity that exist between domains with different orientations in film G120B.

D. Comparison with the behavior of Josephson junctions based on artificial grain boundaries

Josephson junctions based on pair tunneling across an artificial grain boundary between domains with the same basal plane have been extensively studied. The angle between the domains determines the behavior of the junctions. According to Horide and co-workers,[31,32] below 2° the current-voltage curves show that Abrikosov vortices are in motion in the flux flow regime along the grain boundary, while Abrikosov-Josephson vortices flow along grain boundaries with an angle between 2° and 8°. The artificial grain boundaries behave as Josephson junctions for angles larger than 10°. At the difference from the devices including artificial grain boundaries, the angle between the connected domains has a possible influence on the behavior of microbridges G120B and G123B in the near vicinity of T_c only since the films are in the flux creep regime at lower temperatures. Near T_c however, Fraunhofer or SQUID-like $I_{cr}(B)$ curves were only obtained with the microbridge that includes boundary planes between [100] and [110] domains (microbridge G120B). From another point of view, the sensitivity of the investigated microbridges to the magnetic field is low, as compared to that of samples including artificial grain boundaries with a similar size. This can be attributed to the value of ℓ_c that is in the range of the short modulating structures shown in Fig. 1, while in high angle artificial grain boundaries the coherence length in Ψ can extend over the whole length of the grain boundary.

VI. CONCLUSION

In this contribution we have reported critical current measurements carried out in low applied magnetic fields on two YBCO thin films patterned as microbridges. A Josephson-like modulation of the critical current has been observed in the vicinity of T_c. We have assumed that the modulating structures either consist of n_c successive superconducting weak links or are SQUID-like structures including $2n_c$ superconducting and n_{ns} nonsuperconducting weak links. We have reproduced the measurements using expressions describing the Josephson behavior of these structures, taking into account that disorder exists in the boundary planes. The proximity to T_c of the domain of temperature, in which the reported effects take place, is probably unacceptable for applications. This difficulty could be overcome by making devices with a width smaller than the vortex separation, i.e., by making nanobridges. As mentioned in the introduction, Josephson effects have been effectively observed in nanobridges, but the physics of these devices is different from that of the microbridges and the role of the boundary planes is not clear yet.[10,11,33]

The good agreement between the models and the experimental measurements reported in this contribution is consistent with the suggestion that the natural boundary planes in YBCO films include weak links rows that play a major role in their superconducting properties. Although more work is needed to make this role perfectly clear, the optimization of the devices based on these films requires probably to take this aspect into account.

[1] G. Deutscher and K. A. Müller, Phys. Rev. Lett. **59**, 1745 (1987).
[2] G. Deutscher, IBM J. Res. Dev. **33**, 293 (1989).
[3] J. Halbritter, Phys. Rev. B **48**, 9735 (1993).
[4] E. Mezzetti, R. Gerbaldo, G. Ghigo, L. Gozzelino, B. Minetti, C. Camerlingo, A. Monaco, G. Cuttone, and A. Rovelli, Phys. Rev. B **60**, 7623 (1999).
[5] A. Gurevich, Phys. Rev. B **46**, 3187 (1992).
[6] A. Gurevich and L. D. Cooley, Phys. Rev. B **50**, 13563 (1994).
[7] L. N. Bulaevskii, J. R. Clem, and L. I. Glazman, Phys. Rev. B **46**, 350 (1992).
[8] R. L. Peterson and J. W. Ekin, Phys. Rev. B **37**, 9848 (1988).
[9] T. S. Orlova, J. Y. Laval, and B. I. Smirnov, Mater. Phys. Mech. **1**, 39 (2000).
[10] J. R. Wendt, C. P. Tigges, V. M. Hietala, Th. A. Plut, J. S. Martens, K. Char, and M. E. Johansson, Sandia National Laboratories, Sandia Report No. SAND94-158, 1994 (unpublished).
[11] Johannes Eisenmenger, Frank-Michael Kamm, Alfred Plettl, and Paul Ziemann, Physica C **411**, 136 (2004).
[12] R. Unger, T. A. Scherer, W. Jutzi, Z. G. Ivanov, and E. A. Stepantsov, Physica C **241**, 316 (1995).
[13] C. Camerlingo, M. P. Lissitski, C. Nappi, and M. Russo, Physica C **372-376**, 91 (2002).
[14] Z. Hao, Y. Enomoto, Y. Wu, and K. Tanabe, Physica C **378-381**, 1334 (2002).
[15] F. Lombardi, F. Tafuri, F. Ricci, F. Miletto Granozio, A. Barone, G. Testa, E. Sarnelli, J. R. Kirtley, and C. C. Tsuei, Phys. Rev. Lett. **89**, 207001 (2002).
[16] F. Tafuri, F. Miletto Granozio, F. Carillo, A. Di Chiara, K. Verbist, and G. Van Tendeloo, Phys. Rev. B **59**, 11523 (1999).

[17] P. Bernstein and J. F. Hamet, J. Appl. Phys. **95**, 2569 (2004).
[18] P. Bernstein, J. F. Hamet, M. T. González, and M. Ruibal Acuña, Physica C **455**, 1 (2007).
[19] P. Bernstein, J. F. Hamet, and Y. Thimont, Physica C **468**, 200 (2008).
[20] Y. Zhu, M. Suenaga, J. Tafto, and D. O. Welch, Phys. Rev. B **44**, 2871 (1991).
[21] C. Goupil, F. Warmont, M. Hervieu, J. F. Hamet, and Ch. Simon, Phys. Rev. B **60**, 1418 (1999).
[22] N. D. Browning, J. P. Buban, C. Prouteau, G. Duscher, and S. J. Pennycook, Micron **30**, 425 (1999).
[23] M. E. Gaevski, A. V. Bobyl, D. V. Shantsev, Y. M. Galperin, T. H. Johansen, M. Baziljevich, H. Bratsberg, and S. F. Karmanenko, Phys. Rev. B **59**, 9655 (1999).
[24] R. J. Wijngaarden, R. Griessen, J. Fendrich, and W. K. Kwok, Phys. Rev. B **55**, 3268 (1997).
[25] Antonio Barone and Gianfranco Paternò, *Physics and Applications of the Josephson Effect* (Wiley, New York, 1982), p. 94.
[26] Y. Gao, K. L. Merkle, G. Bai, H. L. M. Chang, and D. J. Lam, Ultramicroscopy **37**, 326 (1991).
[27] C. Prouteau, J. F. Hamet, B. Mercey, M. Hervieu, B. Raveau, D. Robbes, L. Coudrier, and G. Ben-Assayag, Physica C **248**, 108 (1995).
[28] S. M. Anlage, B. W. Langley, G. Deutscher, J. Halbritter, and M. R. Beasley, Phys. Rev. B **44**, 9764 (1991).
[29] D. A. Bonn, Ruixing Liang, T. M. Riseman, D. J. Baar, D. C. Morgan, Kuan Zhang, P. Dosanjh, T. L. Duty, A. MacFarlane, G. D. Morris, J. H. Brewer, W. N. Hardy, C. Kallin and A. J. Berlinsky, Phys. Rev. B **47**, 11314 (1993).
[30] J. Albrecht, S. Leonhardt, and H. Kronmüller, Phys. Rev. B **63**, 014507 (2000).
[31] T. Horide, K. Matsumoto, A. Ichinose, M. Mukaida, Y. Yoshida, and S. Horii, Phys. Rev. B **75**, 020504(R) (2007).
[32] T. Horide, K. Matsumoto, Y. Yoshida, M. Mukaida, A. Ichinose, and S. Horii, Phys. Rev. B **77**, 132502 (2008).
[33] Ch. Peroz, J. C. Villégier, A. F. Dégardin, B. Guillet, and A. J. Kreisler, Appl. Phys. Lett. **89**, 142502 (2006).